

Activating [4+4] photoreactivity in the solid-state via complexation: from 9-(methylaminomethyl)anthracene to its silver(I) complexes.

Received 00th January 20xx,
Accepted 00th January 20xx

DOI: 10.1039/x0xx00000x

www.rsc.org/

Floriana Spinelli,^a Simone d' Agostino^a, Paola Taddei^{*b}, Christopher D. Jones^c, Jonathan W. Steed^c and Fabrizia Grepioni^{*a}

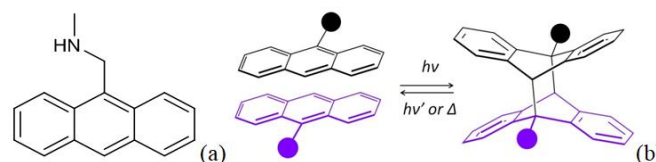
The [4+4] photoreactivity of the anthracene derivative 9-(methylaminomethyl)anthracene (MAMA) has been investigated in solution, gel medium and in the solid state. While quantitative formation of the cycloaddition photoproduct was achieved upon irradiation at $\lambda = 365$ nm of ethanol solutions of MAMA, only partial and slow conversion was detected in gels of low molecular weight gelators, and solid-state reactivity was not observed due to the unfavourable relative orientation of the anthracene moieties in the crystal. In hexafluorophosphate, tetrafluoroborate and nitrate silver(I) complexes, however, 9-(methylaminomethyl)anthracene exhibits a more favourable mutual orientation for the aromatic fragments, and [4+4] photoreactivity resulted. All compounds were structurally characterized via single crystal and/or X-ray powder diffraction and by Raman spectroscopy; this last technique proved effective in detection of the photoproduct in all solid state complexes.

Introduction

In the last few decades crystal engineering, i.e. the design and synthesis of crystalline materials with predefined properties, has attracted the attention of many researchers working in the field of solid-state photoreactivity,^{1,2} as it represents a powerful tool for the modification of crystal properties.³ The correlation between the crystal packing of organic molecules and their photoreactivity (or potential light-stability) was investigated by Schmidt more than 50 years ago. Schmidt studied the [2+2] photoreactivity of cinnamic acid in the solid state, and concluded that "photoreactivity of the cinnamic acid is crystal-structure dependent".⁴ Schmidt proposed his well-known topochemical postulate, which states that photodimerization is expected to take place if the distance between the double bonds involved in the reaction is in the range 3.6–4.1 Å.⁵ In order to show photoreactivity in the solid state, therefore, a crystal should be *engineered* in such a way as to possess appropriate intermolecular alignment and distances.⁴ In order to correctly lock molecules in place within a crystal, to promote photoreactivity and activate photostable molecules,

for [2+2] photodimerization processes salt formation,⁶ the use of molecular templates,⁷ and coordination to metal ions⁸ have all been explored. Photoreactivity of the [4+4] type has also been studied extensively in the case of anthracene and anthracene derivatives.⁹ According to the literature, [4+4] photoreactions usually take place when an optimum superimposition of the π -systems is present, i.e. when certain geometrical criteria¹⁰ - in addition to those in Schmidt's postulate - are fulfilled. However, a large number of exceptions, both positive and negative, have been reported.¹¹ When studying the photoreactivity of anthracene derivatives, the steric effects and the electronic properties of the substituents on the central ring have to be taken into account, since the reaction usually involves the double bonds within this ring. Similarities and differences between [2+2] and [4+4] photodimerizations have been the subject of previous work.^{10,12}

In this work we have investigated the [4+4] photoreactivity of the anthracene derivative 9-(methylaminomethyl)anthracene (MAMA), both in solution and in a supramolecular gel medium (Scheme 1).



Scheme 1 (a) Molecular structure of MAMA; (b) typical photochemical dimerization of 9-substituted anthracenes.

^a Dipartimento di Chimica "Giacomo Ciamician", Università di Bologna, Via Selmi 2, 40126 Bologna, Italy.

^b Dipartimento di Scienze Biomediche e Neuromotorie, Università di Bologna, Via Belmeloro 8/2, 40126 Bologna, Italy.

^c Department of Chemistry, University of Durham, South Road, DH1 3LE, Durham, UK.

†Electronic Supplementary Information (ESI) available: CIF files, table of crystal data, X-ray powder diffraction patterns, synthesis of the bis(urea) gelator, Raman spectra. CCDC 1813325–1813330. For ESI and crystallographic data in CIF or other electronic format see DOI: 10.1039/x0xx00000x

The [4+4] reactivity was also investigated in the solid state on the pure compound, however the material proved photostable. Therefore we have exploited the coordination ability of the MAMA amino group to silver(I) ions, and we have synthesized the silver(I) complexes $[\text{Ag}(\text{MAMA})_2][\text{PF}_6]$, $[\text{Ag}(\text{MAMA})_2][\text{BF}_4]$ and the coordination polymer $[\text{Ag}(\text{MAMA})_2][\text{Ag}(\text{NO}_3)_2]$, in which the relative arrangement of the anthracene derivatives allows the [4+4] photoreaction to occur in the solid state. All solids have been fully characterized via X-ray diffraction and Raman spectroscopy, and the photoreactivity of all coordination compounds investigated and compared with the behaviour of the pure ligand.

Experimental

All reagents were purchased from Sigma-Aldrich and used without further purification. Reagent grade solvents and bidistilled water were used. The gelator G1 (see ESI) was prepared by reaction of *n*-butylamine with 1,3-bis(1-isocyanato-1-methylethyl)benzene. Full characterisation of this compound and its gels are reported elsewhere.¹³

Synthesis and crystal growth of trans-bis-9-methylaminomethyl-9,10-dihydro-9,10-anthracenediyl (DMAMA).

A saturated solution of MAMA obtained by dissolving 100 mg of MAMA in 8 mL of ethanol, and filtering the undissolved solid with a 2 μm pore size filter, was irradiated ($\lambda = 365 \text{ nm}$) in a quartz cuvette for 24 h. After this time yellow crystals appeared (see Fig. S1), which were recovered by filtration, yielding ca. 40 mg of a compound that was identified as trans-bis-9-methylaminomethyl-9,10-dihydro-9,10-anthracenediyl (DMAMA) (see Fig. 1).

Synthesis and crystal growth of the complexes $[\text{Ag}(\text{MAMA})_2][\text{PF}_6]$, $[\text{Ag}(\text{MAMA})_2][\text{BF}_4]$ and $[\text{Ag}(\text{MAMA})_2][\text{Ag}(\text{NO}_3)_2]$.

An amount (104.2 mg; 0.47 mmol) of ligand MAMA was dissolved in 10 mL of ethanol, then an equivalent amount of an AgX salt ($\text{X}^- = \text{PF}_6^-$, BF_4^- or NO_3^-) dissolved in EtOH (4 mL) was added. After a few minutes a yellow precipitate was obtained in all cases; the suspensions were kept under stirring for 24 h, and polycrystalline powders were collected by vacuum filtration and washed with cold EtOH (5 \times 2 mL). Single crystals suitable for X-ray diffraction analysis were grown by triple layer liquid diffusion: a solution of MAMA in ethanol was placed at the bottom of an NMR test tube, and on this a second layer of pure ethanol was deposited, followed by an ethanol solution of the silver salt. The identity between the precipitated materials and single crystals was verified by comparing experimental and simulated powder diffraction patterns (see Fig. S2).

Single crystal X-ray diffraction.

Single crystal data for all complexes were collected at RT on an Oxford X'Calibur S CCD diffractometer equipped with a graphite monochromator (Mo-K α radiation, $\lambda = 0.71073 \text{ \AA}$),

while single crystals of trans-Bis-9-methylaminomethyl-9,10-dihydro-9,10-anthracenediyl (DMAMA) were collected on a Bruker D8Venture diffractometer (PHOTON-100 CMOS_detector, μS -microsource, focusing mirrors, Mo-K α , $\lambda = 0.71073 \text{ \AA}$) and processed using Bruker APEX-II software. Data collection and refinement details are listed in Table S1. All non-hydrogen atoms were refined anisotropically. CH hydrogen atoms for all complexes were added in calculated positions and refined riding on their respective carbon atoms; NH hydrogen atoms were either directly located or, when not possible, added in calculated positions. The SHELX97^{14a} programs were used for structure solution and refinement on F^2 . The program Mercury^{14b} was used to calculate intermolecular interactions. CYLview^{14c} and Mercury^{14b} were used for molecular graphics. Crystal data can be obtained free of charge via www.ccdc.cam.ac.uk/conts/retrieving.html (or from the Cambridge Crystallographic Data Centre, 12 Union Road, Cambridge CB21EZ, UK; fax: (+44)1223-336-033; or e-mail: deposit@ccdc.cam.ac.uk). CCDC numbers 1813325-1813330 (see crystallographic details in Table S1).

Structure determination and refinement of MAMA from X-ray powder data.

Recrystallization of MAMA from melt afforded a polycrystalline powder, which allowed the structure solution from powder X-ray diffraction data (see Fig. S3). For structure solution and refinement purposes, X-ray powder diffractograms in the 2θ range 3–70° (step size, 0.013°; time/step, 172s; 0.02 rad s⁻¹; $V \times A$ 40 \times 40) were collected on a Panalytical X'Pert PRO automated diffractometer operated in transmission mode (capillary spinner) and equipped with a Pixel detector; three patterns were recorded and summed to enhance the signal to noise ratio. Powder diffraction data were analysed with the software EXPO2014,^{15a} which is designed to analyse both monochromatic and non-monochromatic data. Peaks were automatically chosen in the 2θ range 5–50°, and a triclinic cell with a volume of 1242.2 Å^3 (Table S1) was found using the algorithm N-TREOR.^{15b} The structure was then solved by simulated annealing using a molecular model built with the Avogadro software,¹⁶ and refined as rigid body by Rietveld method with the software TOPAS 4.1.¹⁷ A shifted Chebyshev function with 6 parameters and a Pseudo-Voigt function (TCHZ type) were used to fit background and peak shape, respectively. A spherical harmonics model was used to describe the preferred orientation. A rigid body was applied on the two fragments. An overall thermal parameter for the C, N, O atoms was adopted. The H_{NH} atom is disordered over two equivalent positions. Refinement converged with GOF = 3.7, Rwp = 8.1%, Rexp = 2.2%.

X-ray powder diffraction.

For phase identification purposes X-ray powder diffractograms in the 2θ range 5–80° (step size, 0.02°; time/step, 20 s; 0.04 rad s⁻¹; 40mA \times 40kV) were collected on a Panalytical X'Pert PRO automated diffractometer equipped with an X'Celerator detector and in Bragg-Brentano geometry, using Cu K α

radiation without a monochromator. The program Mercury^{14b} was used for simulation of X-ray powder patterns on the basis of single crystal data. Chemical and structural identity between bulk materials and single crystals was always verified by comparing experimental and simulated powder diffraction patterns (see Fig. S2).

Solid State Photoreactions.

In all cases irradiation was performed using a UV-LED (Led Engin LZ1-10UV00-0000), at $\lambda = 365$ nm. A saturated ethanolic solution of 9-(methylaminomethyl)anthracene (MAMA) was placed in a quartz cuvette and irradiated using two UV-LEDs placed at a distance of 2 cm from the cuvette. Single crystal samples were irradiated placing the UV-LED at a distance of 1 cm. Powder samples were placed onto a flat sample holder and irradiated keeping the LED at a distance of 2 cm. For complexes $[\text{Ag}(\text{MAMA})_2][\text{BF}_4]$ and $[\text{Ag}(\text{MAMA})_2][\text{Ag}(\text{NO}_3)_2]$ the XRPD patterns run before and after irradiation are reported in Fig. S4.

Raman spectroscopy

Raman spectra were recorded on a Bruker MultiRam FT-Raman spectrometer equipped with a cooled Ge-diode detector. The excitation source was an Nd³⁺-YAG laser (1064 nm) in the backscattering (180°) configuration. The focused laser beam diameter was about 100 μm and the spectral resolution 4 cm^{-1} . Laser power at the sample was about 30 mW for unirradiated samples and irradiated MAMA and 1 mW for the irradiated complexes due to the high fluorescence background. The spectra of the latter samples were baseline corrected. Under these conditions no photodegradation of the samples was detected.

Gel phase crystallization

A total of 10 mg of bis(urea) gelator G1 and 8 mg of anthracene or MAMA were suspended in 1 mL of toluene. Upon heating with a heat gun a clear solution was obtained, and a gel formed on cooling within a few minutes. The gel was irradiated at 365 nm overnight resulting in large crystals of the anthracene photoproduct within the gel (Fig S5b). In order to recover the crystals of the photoproduct, the gel was decomposed with a 2% ethanol solution of tetrabutylammonium acetate, allowing recovery of the crystals by filtration (Fig. S5a). No solid product was obtained in the case of MAMA.

Results and discussion

[4+4] photoreactivity of MAMA

The photoreactivity of 9-(methylaminomethyl)anthracene (MAMA) was first investigated in solution. A solution of MAMA in ethanol was irradiated with UV light at $\lambda = 365$ nm: after 15 h an insoluble product, in the form of crystalline powder, was recovered.

The formation of the dimer was confirmed by X-ray diffraction. Fig. 1a shows the molecular structure of the dimer DMAMA formed by MAMA photodimerization; Fig. 1b shows how the amino groups on adjacent molecules are linked in the crystal via long hydrogen bonds of the N(H)⋯N type [$\text{N}\cdots\text{N}$ distance 3.056(2) Å].

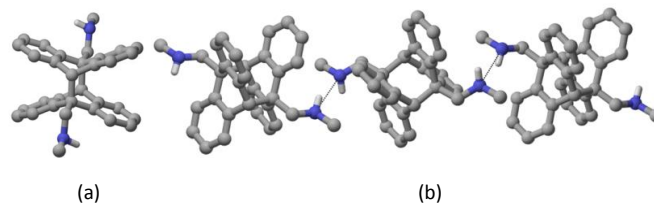


Fig.1 (a) Crystal structure of the photoproduct of the reaction conducted in solution (DMAMA) and b) relevant hydrogen bonding interactions involving the amino groups. H_{CH} omitted for clarity.

The photobehaviour of MAMA was also investigated in the solid state. A polycrystalline sample of MAMA was irradiated at $\lambda = 365$ nm, and powder patterns measured before and after UV exposure: the absence of changes in the diffraction pattern (see Fig. 2) indicates that the compound is photostable.

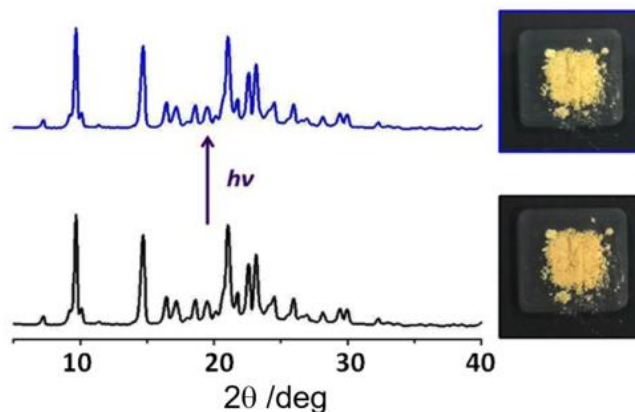


Fig. 2 X-ray powder diffraction patterns recorded before and after UV irradiation at $\lambda = 365$ nm on a polycrystalline sample of pure MAMA.

The photostability may be rationalized by the crystal structure of MAMA. As no coordinates were available in the Cambridge Structural Database, growth of good quality single crystals was attempted (i) by solution crystallization (from ethanol, methanol, dichloromethane, chloroform, toluene), ii) via different crystallization techniques, e.g. solvent evaporation, liquid diffusion or vapour diffusion, iii) from gels of low-molecular-weight gelators (LMWG)¹⁸, iv) from the melt. While all attempts to obtain single crystals suitable for X-ray diffraction were unsuccessful, recrystallization from the melt afforded a good quality polycrystalline powder; structure solution for MAMA was thus possible from powder X-ray diffraction data (see Table S1 and Fig. S3). Fig. 3 shows the structure of crystalline MAMA. In comparison to the structure of the photodimer (Fig. 1), the same pairing of molecules is evident, but the N(H)⋯N separation is much larger [$\text{N}\cdots\text{N} =$

3.321(1) Å] and the relative arrangement of the aromatic rings, with displaced double bonds in a herring-bone pattern, does not favour the photodimerization reaction (see Table 1). As a consequence, crystalline MAMA is photostable.

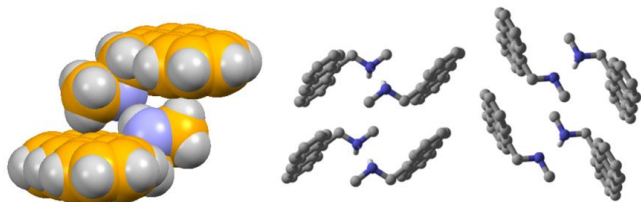


Fig. 3 Molecular pairs arrangement in crystalline MAMA and herring-bone pattern (compare with DMAMA in Fig. 1). H_{CH} omitted for clarity.

Attempts were also made to use low molecular weight organogels as media for photocrystallization of MAMA, and anthracene as a control. The anthracene and MAMA were dissolved in hot toluene in the presence of 1 wt% of the bis(urea) gelator G1 (see Fig. 4 and ESI).¹³ Transparent gels formed within a few minutes upon cooling and the samples were irradiated overnight at 365nm alongside a solution control. The anthracene gel sample yielded large crystals of the dianthracene photoproduct. Consistent with their formation in a gel medium the lack of convection currents¹⁹ resulted in larger, better-formed crystals than the solution control (see Figs. 4 and S6).

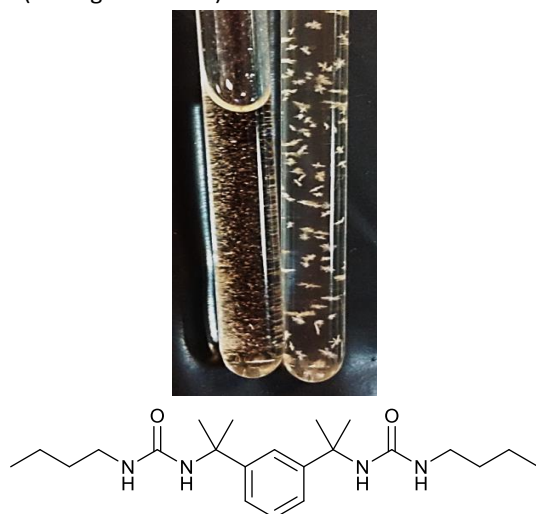


Fig. 4 Top: Comparison of crystals of the dimer of anthracene obtained, after irradiation, in solution (left) and in a supramolecular gel medium (right). Bottom: the bis(urea) gelator G1.

Subsequent treatment of the gel with a solution of ethanolic tetrabutylammonium acetate resulted in gel dissolution, allowing recovery of the crystals by filtration (Fig. S5a). Interestingly, for MAMA in contrast to the solution experiment in which photoreactivity was detected after a few minutes, no photoproduct was formed in the gel in the first seven hours of irradiation (see Fig. S6). This result implies that the MAMA environment in the gel is solid-like and the MAMA molecules are held apart from one another in an orientation that is unfavourable for photodimerisation, possibly by absorption

onto the gel fibres. Monitoring the reaction using ¹H NMR spectroscopy shows evidence for very slow, partial conversion to the photodimer (see supplementary information).

Turning MAMA into a ligand: coordination to silver(I)

The photostability of MAMA in the solid state depends on the relative arrangement of the anthracene moieties. This can in principle be modified and a favourable geometry obtained by coordination to metal ions. Examples can be found in the literature in the case of [2+2] photocycloadditions,²⁰ but, to the authors' knowledge, this approach has never been tried with anthracene derivatives. We reacted MAMA with silver(I) salts and obtained solids in which, due to coordination to the metal ions, the potentially reactive groups could be locked in place in a favourable geometric arrangement. Direct reaction in solution between MAMA and the silver(I) salts resulted in the formation of the complexes [Ag(MAMA)₂][PF₆], [Ag(MAMA)₂][BF₄] and [Ag(MAMA)₂][Ag(NO₃)₂], irrespective of the stoichiometric ratio used for the reagents. The possibility of obtaining the same complexes via mechanochemistry²¹ (manual grinding/kneading or ball-milling) was also explored, but no complex formation was detected in all cases.

The complexes [Ag(MAMA)₂][PF₆] and [Ag(MAMA)₂][BF₄] (see Figs. 5a and 5b, respectively) are isomorphous, and both crystallize in the monoclinic space group C2/c (Table S1), while the molecular salt [Ag(MAMA)₂][Ag(NO₃)₂], which also crystallizes in C2/c, is characterized by a different packing arrangement.

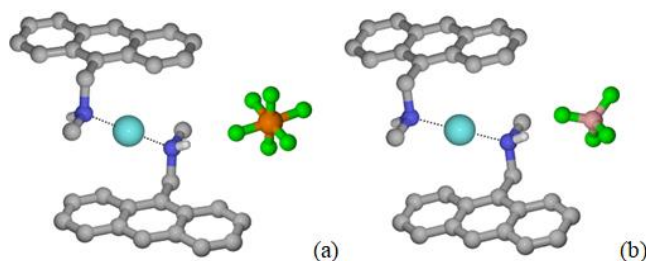


Fig. 5 The formula unit in crystalline [Ag(MAMA)₂][PF₆] (a) and [Ag(MAMA)₂][BF₄] (b), showing the coordination of the MAMA ligands around the silver(I) cation (in light blue) and the inorganic counterion. Silver ions enlarged, H_{CH} omitted for clarity.

In both the hexafluorophosphate and tetrafluoroborate salts the [Ag(MAMA)₂]⁺ ion can be described as a 0D complex, consisting of two MAMA molecules coordinated to silver(I) in a linear fashion [N–Ag⁺ 2.165(1) and 2.177(1) Å for [Ag(MAMA)₂][PF₆] and [Ag(MAMA)₂][BF₄], respectively, with the silver cation on a crystallographic centre of inversion]. In crystalline [Ag(MAMA)₂][Ag(NO₃)₂], while the cation remains the same [N–Ag⁺ = 2.178(1) Å], the counterion is a silver(I) dinitrate complex, formed by the coordination of two nitrate anions to silver(I) via two oxygen atoms per NO₃[−] unit [O–Ag⁺ = 2.447(1) Å, see Fig. 6]. The silver ion belonging to the anionic complex also participates in Ag⁺⋯π interactions [η¹ = 2.712(1) Å] with the aromatic rings on neighboring cations,²² thus resulting in the formation of a 1D coordination polymer (see Fig. 6) extending along the c-axis direction.

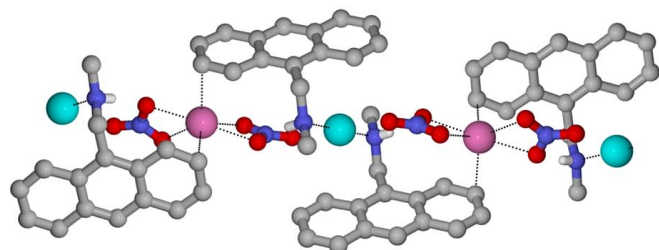
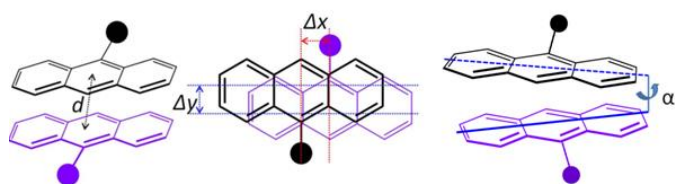


Fig. 6 The 1D coordination polymer in crystalline $[\text{Ag}(\text{MAMA})_2][\text{Ag}(\text{NO}_3)_2]$, showing how the two silver complexes (Ag^+ cation in light blue, Ag^+ anion in pink) are linked to each other via $\eta^2\text{-MAMA}\cdots\text{Ag}^+$ interactions. Silver ions enlarged, H_{CH} omitted for clarity.

Scheme 2 lists the common criteria used to estimate, on the basis of purely geometrical parameters, the feasibility of a [4+4] photoreaction in the solid state.



Scheme 2 Geometrical parameters used to evaluate the potential solid state photoreactivity of the MAMA ligand in its silver(I) complexes; only ligands facing each other at close distance are considered. From left to right: d = distance between centroids; Δy and Δx = transversal and longitudinal offset; α = dihedral angle formed by the long molecular axes.

The most interesting feature, common to the three crystalline materials, is the presence of pairs of MAMA ligands facing each other in a head-to-tail fashion (see Fig. 7).

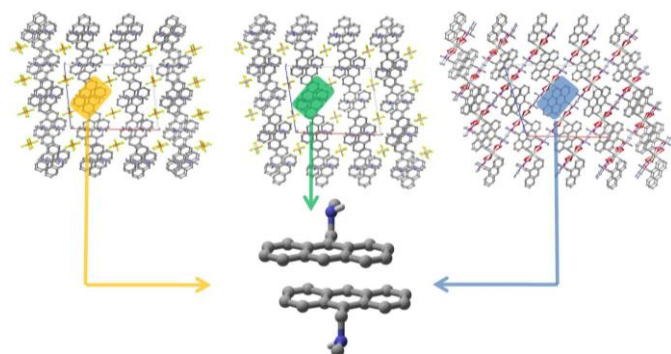


Fig. 7 Projections in the ac -planes of crystalline $[\text{Ag}(\text{MAMA})_2][\text{PF}_6]$ (left), $[\text{Ag}(\text{MAMA})_2][\text{BF}_4]$ (middle) and $[\text{Ag}(\text{MAMA})_2][\text{Ag}(\text{NO}_3)_2]$ (right): the yellow, green and blue rectangles evidence the anthracene pairs (bottom) common to all packings.

Table 1 lists the geometrical parameters, described in Scheme 2, for pure MAMA and for the three complex salts: distances and angular values all indicate that in the case of the complexes a [4+4] photodimerization reaction should be a feasible process.

Table 1 Relevant geometrical parameters used for the evaluation of potential solid state photoreactivity.

	d (Å)	Δx (Å)	Δy (Å)	α (°)
MAMA	5.481(9)	2.262(2)	3.406(9)	0
$[\text{Ag}(\text{MAMA})_2][\text{PF}_6]$	3.701(1)	0.954(1)	1.083(3)	0
$[\text{Ag}(\text{MAMA})_2][\text{BF}_4]$	3.691(1)	0.211(1)	1.332(4)	0
$[\text{Ag}(\text{MAMA})_2][\text{Ag}(\text{NO}_3)_2]$	3.819(9)	1.563(2)	0.801(1)	0

UV irradiation experiments on the crystalline complexes were first conducted on the same single crystals used for data collection and structural determination. Upon UV irradiation, however, in all three cases the single crystals “crumbled”. The effect of the UV irradiation on a single crystal of $[\text{Ag}(\text{MAMA})_2][\text{PF}_6]$ can be seen in Fig. 8. It is worth noting that the tiny residual, pale yellow single crystals (Fig. 8c) were identified as the starting material, therefore the reaction was incomplete, probably due to inhomogeneous or inefficient permeation of the UV radiation. The transformation of the crystal into polycrystalline powder must be due to the large internal pressure originated from molecular displacements, as an effect of the [4+4] photodimerization process.²³

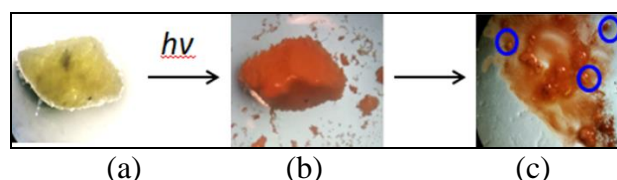


Fig. 8 (a) The single crystal of $[\text{Ag}(\text{MAMA})_2][\text{PF}_6]$ used for crystal structure determination, and optical microscope images taken before (a), during (b) and after (c) UV irradiation. Blue circles indicate residual pale yellow crystalline fragments large enough to be mounted on the diffractometer and identified as starting material.

Photoreactivity of polycrystalline samples was also tested for all compounds, and XRPD patterns were measured for all irradiated samples (see Figs. 9 for $[\text{Ag}(\text{MAMA})_2][\text{PF}_6]$ and S4 in ESI for the other two complexes). Only minor changes were detected for $[\text{Ag}(\text{MAMA})_2][\text{PF}_6]$ (see Fig. 9) with respect to the pattern of the untreated sample, as expected if the photoreaction occurs topotactically, i.e. with symmetry retention.²⁴ The absence of relevant differences in the powder patterns before and after irradiation makes it difficult to distinguish between the product of a topotactic reaction and an unreacted sample. The colour of the polycrystalline sample before and after irradiation is comparable to the colour change observed when a single crystal was employed (Fig. 9).²⁵

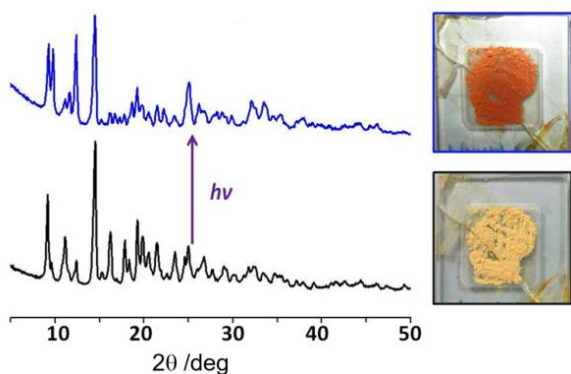


Fig. 9 Powder X-ray diffraction patterns and pictures before (black line) and after (blue line) UV irradiation at $\lambda = 365$ nm of polycrystalline $[\text{Ag}(\text{MAMA})_2][\text{PF}_6]$.

Isolation of the photoproduct

The orange powder obtained after irradiation of polycrystalline $[\text{Ag}(\text{MAMA})_2][\text{PF}_6]$ was tested for the presence of the cycloaddition reaction product, i.e. *trans*-Bis-9-methylaminomethyl-9,10-dihydro-9,10-anthracenediyl (DMAMA). DMAMA was indeed isolated, and the photoreaction confirmed, by treating the irradiated solid with a diluted $\text{HBr}_{(\text{aq})}$ solution; this allowed precipitation and removal by filtration of AgBr . Crystallization of the solution via evaporation yielded a few pale yellow single crystals, which were identified, via single crystal X-ray diffraction, as the bromide salt of the photoproduct $[\text{DMAMAH}_2]\text{Br}_2$ (see Fig. 10).

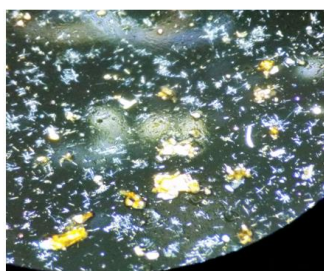


Fig. 10 Single crystals of $[\text{DMAMAH}_2]\text{Br}_2$.

The crystal structure consists of sheets of cations and anions, linked within the planes via charge assisted hydrogen bonds between $[\text{DMAMAH}_2]^{2+}$ and Br^- [$\text{N}^+(\text{H})\cdots\text{Br}^-$ 3.239(6) and 3.330(6) Å] (see Fig. 11).

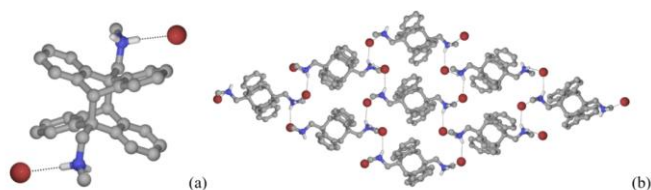


Fig. 11 (a) Molecular structure of crystalline $[\text{DMAMAH}_2]\text{Br}_2$ and (b) the 2D hydrogen bonding network formed by $[\text{DMAMAH}_2]^{2+}$ cations and Br^- anions. H_{CH} omitted for clarity.

The photoconversion process in the $[\text{PF}_6]^-$ and the remaining complexes was further investigated via Raman spectroscopy in

the solid state. The photostability of MAMA was also studied for sake of comparison.

Raman spectroscopy

Fig. 12 shows the Raman spectra of MAMA and DMAMA; their main vibrational bands and assignments are reported in Table S2 (see ESI). Since these Raman spectra have been published here for the first time and no assignments have been reported in the literature for these compounds, anthracene²⁶ and its 9-substituted derivatives^{26d,27} were used as model samples for MAMA, while dianthracene²⁸ photodimers of anthracene derivatives²⁹, 9,10-dihydroanthracene and derivatives³⁰ as well as *ortho*-xylene³¹ were used as model compounds for DMAMA. Many spectral features are characteristic of the dimer; the most prominent are indicated with a circle and their wavenumber positions are in agreement with those reported by Ebisuzaki *et al.* for dianthracene^{28a} see Table S2. The main marker bands of dimerization were identified at 1597-1591, 1085, 1042, 989, 898, 816, 685, 571, 365, 326, 153, 137 cm^{-1} . Interestingly, most of them were also detected and in the IR spectrum of dianthracene.^{28b} Going from MAMA to DMAMA, some bands disappeared or significantly weakened; the strongest were those at 1558 and 1408 cm^{-1} , assignable to aromatic CC ring stretching modes.^{26a} Actually, the weakening of the 1400 cm^{-1} band has been used to follow the photodimerization of anthracene derivatives.³²

As shown in Table S2, several bands specifically assignable to 9-substituted and alkyl-substituted anthracenes (i.e. those at 1625, 1558, 1503-1493, 1408, 1381, 1356, 1101, 972-957, 879, 733, 693, 476, 421, 394 cm^{-1})^{27a,27c-d,28b,31a,33} or fused benzenoid rings (i.e. those at 1408 and 394 cm^{-1})^{26d} were not detected in the Raman spectrum of DMAMA, as expected. In the aromatic CH out of plane bending region, the 879 cm^{-1} component, assigned to the CH group approximately perpendicular to the longer axis of the molecule (i.e. at the 10 position^{28b}), was no longer observed in the spectrum of DMAMA, since the C-H bond at the 10 position is now not aromatic in this molecule; on the other hand, the 750 cm^{-1} component, due to the CH groups approximately parallel to the longer axis of the molecule,^{28b} did not disappear in the spectrum of DMAMA and became more prominent due to the contribution of the CH out of plane bending of *ortho*-disubstituted benzenes.^{28b} Upon irradiation of MAMA, no dimerization occurred; as shown in Fig. S7, the dimerization marker bands described above were not detected. Only minor changes were observed upon irradiation, ascribable to slight molecular rearrangements. No photodegradation of the sample occurred and no production of anthraquinone species was observed and their main marker band at about 1660 cm^{-1} (C=O stretching^{34,27d,30c}) was not detected. An analogous result has been reported for 9-N,N-dimethylaminomethylanthracene.^{6c} Figs. S8, S9 and S10 show the Raman spectra of the $[\text{Ag}(\text{MAMA})_2][\text{BF}_4]$, $[\text{Ag}(\text{MAMA})_2][\text{PF}_6]$ and $[\text{Ag}(\text{MAMA})_2][\text{Ag}(\text{NO}_3)_2]$ complexes, respectively; the Raman spectrum of MAMA is reported for comparison. Upon coordination, similar changes were observed in the spectra of the complexes, while some bands

are specifically assignable to the different counterions,³⁵ as indicated in the figures. With regards to $[\text{Ag}(\text{MAMA})_2][\text{Ag}(\text{NO}_3)_2]$ (Fig. S10), the strengthening of the band at 1477 cm^{-1} is assignable to the contribution of the $\text{N}=\text{O}$ stretching mode and is a marker of the NO_3^- bidentate coordination,³⁶ in agreement with the single crystal XRD data. In the spectra of all the complexes, changes in wavenumber positions and relative intensities of several bands assignable to the aromatic system (see Table S2 for assignments) were observed in the CC stretching ($1630\text{--}1400\text{ cm}^{-1}$ range), CH in plane bending ($1400\text{--}1000\text{ cm}^{-1}$ range), CH out of plane ($1000\text{--}700\text{ cm}^{-1}$ range) and ring bending and torsion modes (below 700 cm^{-1}). The wavenumber position of the N-Ag-N symmetric stretching vibration appears controversial; Miles *et al.*³⁷ have reported this mode at 370 cm^{-1} in $[(\text{H}_3\text{N})_2\text{Ag}][\text{ClO}_4]$ and $[(\text{H}_3\text{N})_2\text{Ag}][\text{NO}_3]$. On the contrary, Hildebrandt and Stockburger have observed the Ag-N stretching mode at 232 cm^{-1} when rhodamine 6G (R6G) molecules covalently link to colloidal silver,³⁸ in agreement with previous studies.³⁹ At the same time, depending on the counterion, these authors have detected a band at 356 cm^{-1} , which they assign to bending and torsional vibrations of the carbon skeleton, i.e. to modes extremely sensitive to molecular distortion. Therefore, these authors have suggested that the anion-induced spectral changes may reflect a modified interaction between R6G and silver, claiming a strong coupling between the anion and the Ag-R6G bonds. Analogous trends were observed in the present spectra of the silver complexes: all of them exhibited different intensity bands at about 225 cm^{-1} (Ag-N stretching) and 360 cm^{-1} (bending and torsional vibrations of the carbon skeleton). With regards to $[\text{Ag}(\text{MAMA})_2][\text{Ag}(\text{NO}_3)_2]$, the Ag-O stretching vibrations are expected to occur in the $250\text{--}450\text{ cm}^{-1}$ region.⁴⁰ Figs. 10, 11 and 12 show the Raman spectra of the $[\text{Ag}(\text{MAMA})_2][\text{BF}_4]$, $[\text{Ag}(\text{MAMA})_2][\text{PF}_6]$ and $[\text{Ag}(\text{MAMA})_2][\text{Ag}(\text{NO}_3)_2]$ complexes, respectively, before and after irradiation. It is evident that the spectra of the irradiated samples showed the same bands as the unirradiated ones together with the above mentioned marker bands of dimerization, with decreasing relative intensity going from $[\text{Ag}(\text{MAMA})_2][\text{PF}_6]$ to $[\text{Ag}(\text{MAMA})_2][\text{BF}_4]$ and $[\text{Ag}(\text{MAMA})_2][\text{Ag}(\text{NO}_3)_2]$. In the spectra of all the irradiated complexes, the aromatic CC stretching band at about 1410 cm^{-1} appeared to be of lower intensity with respect to the corresponding spectra recorded before irradiation.

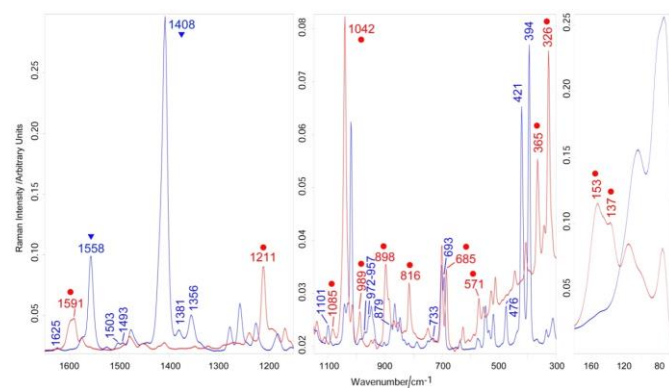


Fig. 12 Raman spectra of MAMA (blue) and DMAMA (red). The main bands characteristic of the dimer are indicated with a circle; the strongest bands that disappear or significantly weakened in the dimer are indicated with a triangle.

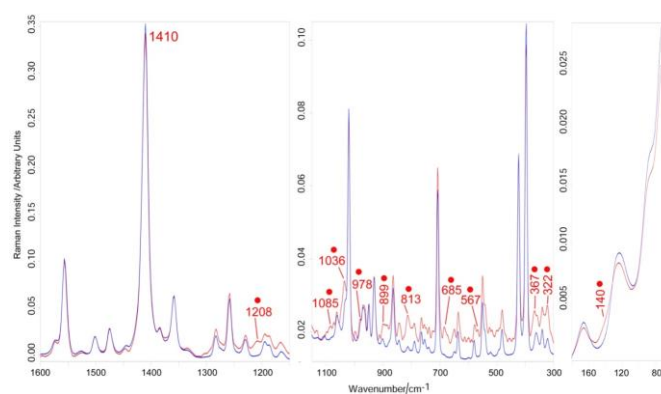


Fig. 13 Raman spectra of $[\text{Ag}(\text{MAMA})_2][\text{BF}_4]$ before (blue) and after irradiation (red). The marker bands of the occurred dimerization are indicated with a circle.

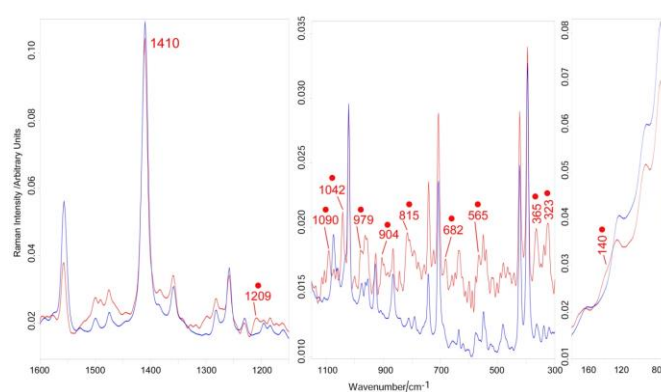


Fig. 14 Raman spectra of $[\text{Ag}(\text{MAMA})_2][\text{PF}_6]$ before (blue) and after irradiation (red). The marker bands of the occurred dimerization are indicated with a circle.

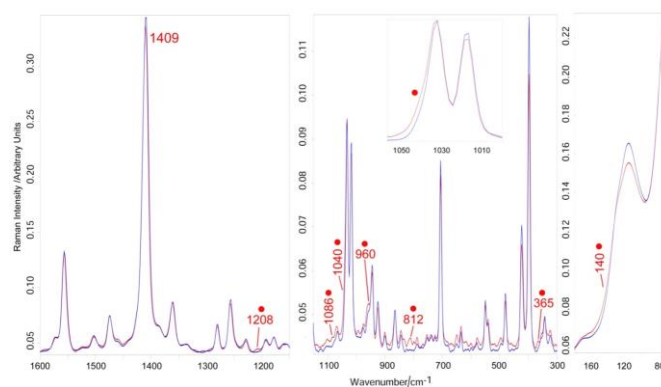


Fig. 15 Raman spectra of $[\text{Ag}(\text{MAMA})_2][\text{Ag}(\text{NO}_3)_2]$ before (blue) and after irradiation (red). The marker bands of the occurred dimerization are indicated with a circle.

Conclusions

In this work we have reported the [4+4] photoreactivity of MAMA in solution, in supramolecular gel medium and in the solid state. Interestingly, the photoreaction in ethanolic solution proceeds uniquely to give the head-to-tail photodimer

DMAMA accompanied also by the growth of crystals suitable for structure determination by X-ray diffraction methods. No reaction was detected in the solid state, on polycrystalline samples of MAMA, and very little reaction occurred in the gel. The lack of photoreactivity in the solid state can be rationalized on the basis of the crystal structure of MAMA, solved from X-ray powder data, which highlighted an unsuitable herringbone packing of MAMA within the crystal. This fact was also confirmed by Raman spectroscopy. The surprising lack of reactivity in the gel implies that MAMA molecule are likewise held in an unfavourable mutual orientation for photoreaction. The photoreactivity of MAMA was also studied in crystalline complexes prepared from reaction between MAMA and three silver salts (AgPF_6 , AgBF_4 , and AgNO_3). Two molecular complexes $[\text{Ag}(\text{MAMA})_2][\text{PF}_6]$, $[\text{Ag}(\text{MAMA})_2][\text{BF}_4]$ and the 1D coordination polymer $[\text{Ag}(\text{MAMA})_2][\text{Ag}(\text{NO}_3)_2]$ were obtained and characterized by means of XRD techniques. Structure determination from single crystal X-ray diffraction has shown, in all of the complexes obtained, that the anthracene-based ligands were properly aligned to undergo a solid state [4+4] photoreaction. Photoreactions were tested firstly on single crystal samples, which evidenced complete degradation into polycrystalline powders in all cases. This phenomenon is ascribed to the tremendous pressure and arising from the atomic/molecular movements within the crystals during the photoreaction. The behavior of polycrystalline samples was also investigated by powder X-ray diffraction and Raman spectroscopy. Raman spectroscopy proved to be a highly effective complementary technique that permitted us to investigate the formation of solid state photoproducts, which were not distinctly defined by XRPD. For the irradiated polycrystalline sample $[\text{Ag}(\text{MAMA})_2][\text{PF}_6]$ we sought crystallographic evidence of the [4+4] photoreaction, i.e. the irradiated solid was treated with diluted solution of HBr. This resulted in the formation of crystals of the hydrobromide salt of the photoproduct, $[\text{DMAMAH}_2]\text{Br}_2$.

Conflicts of interest

There are no conflicts to declare.

Acknowledgements

We acknowledge financial support from the University of Bologna. The Chemistry Department Ciamician is also acknowledged (FS) for a Marco Polo grant. We thank Dr. Dmitry S. Yufit for his help with data collection and structure solution of DMAMA.

Notes and references

- (a) J. O. Metzger, *Angew. Chem., Int. Ed.*, 1998, **37**, 2975; (b) M. D. Cohen and G. M. Schmidt, *J. Chem. Soc.*, 1964, 1996;
- (a) G. Kaupp, in *Making Crystals by Design*, D. Braga and F. Grepioni, WILEY-VCH, Weinheim, 2006, 87–148; (b) K. Biradha and R. Santra, *Chem. Soc. Rev.*, 2013, **42**, 950–967.
- D. Braga, F. Grepioni, L. Maini and S. d'Agostino, *IUCrJ*, 2017, **4**, 369–379.
- G. M. J. Schmidt, *Pure Appl. Chem.*, 1971, **27**, 64.
- G. M. J. Schmidt, *J. Chem. Soc.*, 1964, 2014.
- (a) S. d'Agostino, F. Spinelli, E. Boanini, D. Braga and F. Grepioni, *Chem. Comm.*, 2016, **52**, 1899–1902; (b) S. d'Agostino, P. Taddei, E. Boanini, D. Braga and F. Grepioni, *Cryst. Growth Des.*, 2017, **17**, 4491–4495; (c) H. Ihmels, D. Leusser, M. Pfeiffer and D. Stalke, *Tetrahedron*, 2000, **56**, 6867–6875; (d) M. Horiguchi and Y. Ito, *J. Org. Chem.*, 2006, **71**, 3608–3611.
- (a) L. R. MacGillivray, J. L. Reid and J. A. Ripmeester, *J. Am. Chem. Soc.*, 2000, **122**, 7817–7818. (b) M. Sinnwell and L. R. MacGillivray, *Angew. Chem. Int. Ed.*, 2016, **55**, 3477–3480; (c) D. P. Ericson, Z. P. Zurfluh-Cunningham, R.H. Groeneman, E. Elacqua, E.W. Reinheimer, B. C. Noll and L. R. MacGillivray, *Cryst. Growth Des.*, 2015, **15**, 5744–5748. (d) D. Braga, S. d'Agostino and F. Grepioni, *Cryst. Growth Des.*, 2012, **12**, 4880–4889.
- E. C. Constable, G. Zhang, C. E. Housecroft and J. A. Zampese, *Dalton Trans.*, 2011, **40**, 12146.
- (a) H. Bouas-Laurent, A. Castellán and J. P. Desvergne, *Pure&Appl.Chem.*, 1980, **52**, 2633–2648; (b) G. W. Breton and X. Vang, *J. Chem. Educ.*, 1998, **75**, 81–82; (c) J. Ferguson, *Chem. Rev.*, 1986, **86**, 957.
- I. Zouev, D. Cao, T. V. Sreevidya, M. Telzhensky, M. Botoshansky and M. Kaftory, *CrystEngComm*, 2011, **13**, 4376–4381.
- T. Salzillo, S. Zaccheroni, R. G. Della Valle, E. Venuti and A. Brillante, *J. Phys. Chem. C*, 2014, **118**, 9628–9635.
- I. Turowska-Tyrk and E. Trzop, *Acta Cryst.*, 2003, **B59**, 779–786.
- M. Mirzamami, A. Dawn, H. Kumari, C. D. Jones and J. W. Steed, manuscript in preparation.
- (a) Sheldrick, G. M. SHELX97, Program for Crystal Structure Determination; University of Göttingen: Göttingen, Germany, 1997; (b) C. F. Macrae, I. J. Bruno, J. A. Chisholm, P. R. Edgington, P. McCabe, E. Pidcock, L. Rodriguez-Monge, R. Taylor, J. van de Streek and P. A. Wood, *J. Appl. Crystallogr.*, 2008, **41**, 466; (c) C. Y. Legault, CYLview, Université de Sherbrooke, 2009.
- (a) A. Altomare, C. Cuocci, C. Giacovazzo, A. Moliterni, R. Rizzi, N. Corriero and A. Falcicchio, *J. Appl. Cryst.*, 2013, **46**, 1231–1235; (b) A. Altomare, C. Giacovazzo, A. Moliterni and R. Rizzi, *J. Appl. Crystallogr.*, 2001, **34**, 704.
- Avogadro: an open-source molecular builder and visualization tool. M. D. Hanwell, D. E. Curtis, D. C. Lonie, T. Vandermeersch, E. Zurek and G. R. Hutchison, *J. Cheminf.*, 2012, 47.
- A. Cohelo, TOPAS-Academic, Coelho Software, Brisbane, Australia, 2007.
- (a) J. A. Foster, R. M. Edkins, G. J. Cameron, N. Colgin, K. Fucke, S. Ridgeway, A. G. Crawford, T. B. Marder, A. Beeby, S. L. Cobb and J. W. Steed, *Chem. Eur. J.*, 2014, **20**, 279–291; (b) C. D. Jones, J. W. Steed, *Chem. Soc. Rev.*, 2016, **45**, 6546–6596.
- J. A. Foster, M. M. Piepenbrock, G. O. Lloyd, N. Clarke, J. A. K. Howard and J. W. Steed, *Nat. Chem.*, 2010, **2**, 1037–1043.
- T. D. Hamilton, D. K. Bucar and L. R. MacGillivray, *New J. Chem.*, 2010, **34**, 2400–2402.
- S. L. James, C. J. Adams, C. Bolm, D. Braga, P. Collier, T. Friscic, F. Grepioni, K. D. M. Harris, G. Hyett, W. Jones, A. Krebs, J. Mack, L. Maini, A. G. Orpen, I. P. Parkin, W. C. Shearouse, J. W. Steed and D. C. Waddell, *Chem. Soc. Rev.*, 2012, **41**, 413.
- (a) J. M. Maier, P. Li, J. Hwang, M. D. Smith and Ken D. Shimizu, *J. Am. Chem. Soc.*, 2015, **137**, 8014–8017; (b) E. A.

- Hall Griffith' and E. L. Amma, *J. Am. Chem. Soc.*, 1974, **96**, 743-749.
- 23 (a) G. Kaupp, J. Schmeyers, M. Kato, K. Tanaka, N. Harata and F. Toda, *J. Phys. Org. Chem.*, 2001, **14**, 444; (b) I. Halasz, *Cryst. Growth Des.*, 2010, **10**, 2817; (c) D.-K. Bučar, T. D. Hamilton and L. R. MacGillivray, in *Organic Nanostructures*, ed. J. L. Atwood and J. W. Steed, WILEY-VCH, Weinheim, 2008, 305–315; (d) M. A. Garcia-Garibay, *Angew. Chem. Int. Ed.*, 2007, **46**, 8945–8947; (e) A. Natarajan and B. R. Bhogala, in *Supramolecular Photochemistry*, John Wiley & Sons, Inc., 2011, 175–228.
- 24 (a) K. Biradha and R. Santra, *Chem. Soc. Rev.*, 2013, **42**, 950; (b) G. Wegner, *Pure Appl. Chem.*, 1977, **49**, 443; (c) C. R. Theocharis and W. Jones, Topotactic and topochemical photodimerization of benzylidenecyclopentanones, in *Organic Solid State Chemistry*, ed. G. R. Desiraju, Elsevier, New York, 1987, 47–68.
- 25 The colour change might be due to a photochromic effect associated to the [4+4] cycloaddition reaction, as mentioned for example in: (a) M. W. Urban, Ed. *Handbook of Stimuli-Responsive Materials*, 2011, Ch. 9, p. 223, Wiley-VCH; (b) D. Bailey, N. Seifi and V. E. Williams, *Dyes and Pigments*, 2011, **89**, 313-318.
- 26 (a) N. Abasbegović, N. Vukotić and L. Colombo, *J. Chem. Phys.*, 1964, **41**, 2575-2577; (b) J. Räsänen, F. Stenman, E. Penttinen, *Spectrochim. Acta A*, 1973, **29**, 395-403; (c) W. F. Maddams, I. A. M. Royaud, *Spectrochim. Acta A*, 1990, **46**, 309-314; (d) I. López-Tocón, J. C. Otero, J. F. Arenas, J. V. Garcia-Ramos, S. Sanchez-Cortes, *Anal. Chem.*, 2011, **83**, 2518–2525; (e) F. R. Dollish, W. G. Fateley, F. F. Bentley, Wiley-Interscience, Chichester, 1974; (f) A. Alparone, V. Librando, *Spectrochim. Acta A*, 2012, **89**, 129–136.
- 27 (a) S. Kou, H. Zhou, G. Tang, R. Li, Y. Zhang, J. Zhao and C. Wei, *Spectrochim. Acta A*, 2012, **96**, 768–775; (b) Y. S. Mary, H. T. Varghese, C. Y. Panicker, T. Thiemann, A. A. Al-Saadi, S. A. Popoola, C. Van Alsenoy, Y. Al Jasem, *Spectrochim. Acta A*, 2015, **150**, 533–542; (c) M. Brigodiot and J. M. Lebas, *Spectrochim. Acta A*, 1971, **27**, 1315-1324; (d) L. H. Colthup, S. E. Daly, Wiberley. *Introduction to Infrared and Raman Spectroscopy*. 3rd Edition, Academic Press, San Diego, 1990.
- 28 (a) Y. Ebisuzaki, T. J. Taylor, J. T. Woo, M. Nicol, *Spectrochim. Acta A*, 1977, **73**, 253-264; (b) S. Singh and C. Sandorfy, *Can. J. Chem.*, 1969, **47**, 257-263.
- 29 L. Opilik, P. Payamyar, J. Szczerbinski, A. P. Schütz, M. Servalli, T. Hungerland, A. Dieter Schlüter and R. Zenobi, *ACS Nano*, 2015, **9**, 4252–4259.
- 30 (a) M. Brigodiot and J. M. Lebas, *J. Mol. Struct.*, 1976, **32**, 297-309; (b) K. Morris and J. Laane, *J. Mol. Struct.*, 1997, **413-414**, 13-20; (c) Y. S. Mary, T. S. Yamuna, C. Y. Panicker, H. S. Yathirajan, M. S. Siddegowda, A. A. Al-Saadi, C. Van Alsenoy and J. Ahmad, *Spectrochim. Acta A*, 2015, **135**, 652–661.
- 31 (a) K. S. Pitzer and D. W. Scott, *J. Am. Chem. Soc.*, 1943, **65**, 803-829; (b) F. R. Dollish, W. G. Fateley and F. F. Bentley, *Characteristic Raman frequencies of organic compounds*. Wiley-Interscience, Chichester, 1974.
- 32 Y. B. Zheng, J. L. Payton, T. B. Song, B. K. Pathem, Y. Zhao, H. Ma, Y. Yang, L. Jensen, A. K. Y. Jen, and P. S. Weiss, *Nano Lett.* 2012, **12**, 5362–5368.
- 33 (a) A. Alparone, V. Librando, Y. Panicker, T. Thiemann, A. A. Al-Saadi, S. A. Popoola, C. Van Alsenoy and Y. Al Jasem, *Spectrochim. Acta A*, 2015, **150**, 533–542.
- 34 D. S. Cordeiro and P. Corio, *J. Braz. Chem. Soc.*, 2009, **20**, 80-87.
- 35 (a) K. Nakamoto. *Infrared and Raman spectra of inorganic and coordination compounds. Part A: Theory and Applications in Inorganic Chemistry*. 5th Edition. Wiley Inter-Science, New York, 1997. (b) R. A. Nyquist, C. L. Putzig and M. A. Leugers. *Handbook of Infrared and Raman spectra of inorganic compounds and organic salts*. Academic Press San Diego, 1997.
- 36 K. Nakamoto. *Infrared and Raman spectra of inorganic and coordination compounds. Part B: Applications in Coordination, organometallic and Bioinorganic Chemistry*. 5th Edition. Wiley Inter-Science, New York, 1997.
- 37 G. Miles, J. H. Patterson, C. W. Hobbs, M. J. Hopper, J. Overend and R. S. Tobias, *Inorg. Chem.*, 1968, **7**, 1721-1729.
- 38 P. Hildebrandt and M. Stockburger, *J. Phys. Chem.*, 1984, **88**, 5935-5944.
- 39 S. Venkatesan, Gayle Erdheim, J. R. Lombardi and R. L. Birke, *Surf. Sci.*, 1980, **101**, 387-398.
- 40 J. R. Ferraro and A. Walker, *J. Chem. Phys.*, 1965, **42**, 1273-77.